NANOSYSTEMS:
PHYSICS, CHEMISTRY, MATHEMATICS

Liu Zh., et al. *Nanosystems: Phys. Chem. Math.*, 2024, **15** (1), 104–114.
http://nanojournal.ifmo.ru
DOI 10.17586/2220-8054-2024-15-1-104-114

Original article

Fluorination of Eu-doped layered yttrium hydroxides: the role of anionic composition

Zhanbo Liu[1,a], Svetlana V. Golodukhina[1,2,b], Svetlana V. Kameneva[1,c], Alexey D. Yapryntsev[1,2,d]

[1]Shenzhen MSU-BIT University, Shenzhen, PRC

[2]Kurnakov Institute of General and Inorganic Chemistry of the Russian Academy of Sciences, Moscow, Russia

[a]sdbzlzb@126.com, [b]brightorangedandelion@gmail.com, [c]kamenevasvetlanav@gmail.com, [d]yapryntsev@igic.ras.ru

Corresponding author: Alexey D. Yapryntsev, yapryntsev@igic.ras.ru

PACS 61.66.Fn; 82.39.Wj; 33.50.Dq; 78.30.-j

ABSTRACT The fluorination processes of layered rare-earth hydroxides (LRHs) intercalated with various anions, including organic ones, have been compared for the first time. The fluorination process was investigated for chloride-, nitrate- and 4-sulfobenzoate-intercalated Eu-doped layered yttrium hydroxides by interaction with aqueous solutions of sodium fluoride at 100–150 °C for 2–48 hours. The final product of fluorination in all cases is the hexagonal yttrium hydroxide fluoride (YHF) phase of $Na_yY_{0.95}Eu_{0.05}(OH)_{3+y-x}F_x \cdot mH_2O$ ($x \sim 3$, $y \sim 0.2$) composition. The formation rate of the YHF increases with the interlayer spacing of the Eu-doped layered yttrium hydroxide.

KEYWORDS layered rare-earth hydroxides (LRHs), fluorination, luminescence, ion exchange, topotactic reactions, metal hydroxyfluorides.

ACKNOWLEDGEMENTS This study was supported by the scholarship for young scientists of President of the Russian Federation (SP-3504.2022.4).

FOR CITATION Liu Zh., Golodukhina S.V., Kameneva S.V., Yapryntsev A.D. Fluorination of Eu-doped layered yttrium hydroxides: the role of anionic composition. *Nanosystems: Phys. Chem. Math.*, 2024, **15** (1), 104–114.

1. Introduction

Metal hydroxyfluorides (or metal hydroxide fluoride) are a broad class of compounds, most of which possess low-dimensional structure, semiconducting properties, anisotropic particle morphology, and the presence of a large number of surface acidic/basic centers [1]. These features of metal hydroxyfluorides cause a wide range of their applied properties. For example, transition metal hydroxyfluorides (Co, Zn, Cd, Mn, Ni, Cu, Ti, Cr, etc.) can be applied in photoluminescence, photocatalysis, optoelectronics, gas sensors, supercapacitors, electrocatalysts for water splitting, oxidation catalysis, and ion batteries [1]. Rare-earth hydroxyfluorides are promising for the preparation of luminescent materials with high refractive index and low phonon energy [2–4]. The structure of metal hydroxyfluorides can be regarded as the structure of fluorine-substituted hydroxides or hydroxyl-substituted metal fluorides. Consequently, modification of metals hydroxides [5] or fluorides [6] is common to obtain hydroxyfluorides.

The hydroxyl ion is an effective luminescence quencher [7]. Therefore, eliminating traces of hydroxyl ions is crucial in synthesizing inorganic phosphors. Consequently, a systematic study focusing on the substitution of hydroxyl ions with fluoride ions represents a significant endeavor for understanding the luminescence quenching process and for developing new, efficient phosphors based on rare earth fluorides. A promising precursor for rare-earth hydroxyfluoride synthesis are layered rare-earth hydroxides (LRHs or LREHs), a unique class of anion-exchange inorganic materials discovered in 2006 [8]. The structure of these compounds consists of alternating positively charged metal-hydroxyl layers and negatively charged anion layers [9]. The high mobility of anions in the layers allows for anion exchange at room temperature. The anion exchange ability of LRHs is used to synthesize a variety of other rare-earth compounds: vanadates [10], tungstates [11], phosphates [12, 13], and fluorides [14]. The mechanism of such reactions is considered as dissolution-reprecipitation [11] and topotactic [15–17]. In the latter case, the pseudo-hexagonal arrangement of rare-earth cations is preserved, which allows the directed preparation of given modifications of rare-earth compounds, such as β-$NaYF_4$ [15] and hexagonal $Y(OH)_{3-x}F_x$ [17].

Fluorination of LRHs allows one to obtain a variety of phases of rare-earth fluoride compounds, including $Ln_2(OH)_5F{\cdot}nH_2O$ [14, 18–20], $Ln_2(OH)_4F_2 \cdot 2H_2O$ [21], $Ln(OH)_{3-m}F_m$ [14, 16, 17, 22, 23], LnF_3 [16, 21], MLn_mF_n (M=K, Na, NH_4; Ln = Y, Na, Pr–Lu) [14–16, 23]. The conditions and compositions of fluorinated layered hydroxides are summarized in Table 1. In fluorination reactions, the type of impurity cation (Li^+, K^+, Na^+, NH_4^+) [16], F/Ln ratio (0.1 – 167) [14, 15], temperature (25 – 180 °C) [21], duration (0.1 – 24 h) [21] and pH [16] are varied. The alkali cations participate in the fluorination of LRHs at high concentration of fluorine [16]. Xu et al [16] showed that the ability to incorporate alkali cation into layered yttrium hydroxide with the formation of MY_mF_n decreases in the NH^{4+}, K^+, Na^+,

Li^+ series, as the hydrate radii of these cations increases. The effect of F/Ln ratio on LRH fluorination was investigated by Li et al [14]. The authors consistently obtained $Y_2(OH)_5F{\cdot}nH_2O$, hexagonal $Y(OH)_{1.57}F_{1.43}$, cubic $NH_4RE_3F_{10}$, and finally cubic $NH_4RE_2F_7$ with increasing F/RE molar ratio. The balance between OH- and F- in the coordination sphere of rare-earth during fluorination can be adjusted by changing pH [16]. In the presence of HNO_3, $Y_2(OH)_5NO_3 \cdot nH_2O$ interacts with NH_4F to form YF_3 and $NH_4Y_2F_7$, in the presence of NH_4OH–$Y(OH)_{3-x}F_x$ and $Y_4O(OH)_9NO_3$ [16]. The factors of temperature and duration of fluorination are practically not investigated in the literature. Layered rare-earth hydroxynitrates are usually used to obtain rare-earth fluorides, but there are a few works on fluorination of lanthanum hydroxysulfate [21] and yttrium hydroxychloride [18, 22]. The above-mentioned references do not allow us to unambiguously identify the role of anionic composition on the LRH fluorination process. The anionic composition determines the interlayer distance and the stoichiometry of layered rare-earth hydroxides, so it can play an important role in the process of their fluorination. Moreover, the organic anion can significantly influence the morphology of the formed fluoride phases, acting as a surfactant [24].

In this work, fluorination of Eu-doped layered yttrium hydroxides (LYEuH) intercalated with different anions has been carried out. The influence of the intercalated anion nature on the composition, structure and morphology of fluorination products has been revealed. Both previously used anions (chloride and nitrate anions) in the fluorination reaction and a new organic anion, 4-sulfobenzoate, were chosen as LYEuH's intercalated anions. Special attention is paid to the influence of fluorination duration (2 – 48 h) and temperature (100 – 150 °C) on the products composition and structure.

2. Experimental section

The following reagents were used without additional purification: $Y(NO_3)_3 \cdot 6H_2O$ (Aladdin, 99.5 %), $Eu(NO_3)_3 \cdot 6H_2O$ (Aladdin, 99.9 %), NaCl (Shanghai lingfeng, 99.5 %), ammonia aqueous solution (Xilong scientific, 25%), potassium 4-sulfobenzoate (Aladdin, 95%), $NaNO_3$ (Shanghai lingfeng, 99.0%), and NaF (Shanghai lingfeng, 99.0%). Distilled water was used in all experiments.

To obtain Eu-doped layered yttrium hydroxychloride (Cl-LYEuH), 1 L aqueous solution containing 47.5 g $Y(NO_3)_3 \cdot 6H_2O$, 2.794 g $Eu(NO_3)_3 \cdot 6H_2O$ and 76.3 g NaCl was prepared. Aqueous ammonia solution was added to the prepared solution under constant stirring until pH=7.3. The obtained suspension was refluxed in a round bottom flask for 4 hours. The obtained precipitate was centrifuged, washed three times with water, then dried at 75% humidity over saturated NaCl solution at 60 °C for 10 days.

To obtain Eu-doped layered yttrium hydroxynitrate (NO_3-LYEuH), 0.2 g of Cl–LYEuH was dispersed in 20 mL aqueous solution containing 2.55 g of sodium nitrate and left under constant stirring for 24 hours. The obtained precipitate was centrifuged, washed three times with water, then dried at 60 °C for 24 hours.

To obtain Eu-doped layered yttrium hydroxysulfobenzoate (4sb–LYEuH), 2.4 g of potassium 4-sulfobenzoate was dissolved in 200 mL of water and the resulting solution was adjusted to pH=6.8 with aqueous ammonia solution. 100 mg of Cl–LYEuH was suspended in 30 mL of the 4-sulfobenzoate solution, and the resulting suspension was hydrothermally treated in a 100 mL autoclave at 120 °C for 24 hours. The obtained precipitate was centrifuged, washed three times with water, then dried at 60 °C for 24 hours.

Fluorination of Eu-doped yttrium layered hydroxides was conducted according to the following scheme. Three different mixtures of 50 mL of 0.05 M NaF solution with 100 mg of Cl–LYEuH, or 110 mg of NO_3–LYEuH, or 140 mg of 4sb–LYEuH (F:Ln ratio = 20:1) were prepared in a 100 mL Teflon autoclaves. The resulting suspensions were stirred for 5 minutes at room temperature, followed by hydrothermal treatment at 100 °C or 150 °C for 2 – 48 hours. The obtained precipitate was centrifuged, washed three times with water, then dried at 60 °C for 24 hours.

Powder X-ray diffraction (PXRD) of layered hydroxide samples was carried out by powder X-ray diffraction on a Tonga TDM-10 diffractometer using CoKα radiation, in the range of angles 2θ 5° – 65° with a step of 0.05°. The identification of the obtained phases was performed by comparison with previously obtained experimental diffractograms and with the PDF2 database. The unit cell parameters were refined by the Le-Bail method in MAUD software.

IR spectra were obtained in the mode of attenuated total reflection on an iCAN 9 FTIR spectrometer, using a ZnSe crystal with a resolution of 1 cm^{-1}.

Thermogravimetric analysis of 10 – 14 mg samples was performed on a Mettler Toledo TGA 2 analyzer when heated at a rate of 10K/min in an argon flow.

Microphotographs were obtained by scanning electron microscopy (SEM) on a Carl Zeiss NVision40 workstation with local X-ray spectral microanalysis (EDX). Elemental ratios were determined using INCA software.

Luminescence spectra of the powders were examined on a PerkinElmer FL8500 fluorescence spectrometer with a resolution of 0.1 nm. Excitation spectra were recorded at wavelength λ_{em} = 616 nm, luminescence spectra were recorded at wavelength λ_{ex} = 394 nm.

3. Results and discussion

According to PXRD data (Fig. 1), Cl–LYEuH was obtained without impurities as a single-phase (Fig. 1). The Cl–LYEuH diffractogram was indexed in orthorhombic system in $P2_12_12$ space group according to [25]. The Cl–LYEuH

TABLE 1. Fluorination conditions of layered rare-earth hydroxides according to literature data

Composition of LRHs	Reaction conditions	Composition of products	References
$Ln_2(OH)_5NO_3 \cdot nH_2O$ Ln=Y/Eu or Y/Yb/Er	NH_4F F:Ln= 3 – 167 3 h 25 °C	$Ln_2(OH)_5F$ $Ln(OH)_{1.57}F_{1.43}$ $NH_4Ln_3F_{10}$ $NH_4Ln_2F_7$	[14]
$Y_2(OH)_5NO_3 \cdot nH_2O$: Ln^{3+} Ln=Yb/Er, Yb/Tm	NaF 0.1 – 24 h 180 °C	β-$NaYF_4$:Ln^{3+} (Ln=Yb/Er, Yb/Tm)	[15]
$Y_2(OH)_5NO_3 \cdot nH_2O$: Eu^{3+}, Tb^{3+}	NH_4F+HNO_3+ MOH (M = Li, Na, K) F:Ln=0.5-10 10 h 180 °C	YF_3 MY_mF_n $Y(OH)_{3-m}F_m$	[16]
$Ln_2(OH)_5NO_3 \cdot nH_2O$ Ln = Y, Pr–Lu	NH_4F 1 h 80 °C	$Ln(OH)_{3-m}F_m$	[17]
$Eu_2(OH)_5Cl{\cdot}nH_2O$	NaF 1 h 25 °C	$Ln_2(OH)_5F{\cdot}nH_2O$	[18]
$(Y/Eu)_2(OH)_5NO_3 \cdot nH_2O$	NH_4F F:Ln=0.1 – 0.4 2 h 25 °C	$(Y/Eu)_2(OH)_5F{\cdot}nH_2O$	[19]
$Ln_2(OH)_5NO_3 \cdot nH_2O$ Ln = Y, Pr–Er	KF 12 h 25 °C	$Ln_2(OH)_5F{\cdot}nH_2O$	[20]
$(La_{0.97}RE_{0.01}Yb_{0.02})_2(OH)_4SO_4 \cdot 2H_2O$ (RE = Ho, Er)	NH_4F F:Ln=5 0.5 – 24 h 25, 180 °C	$Ln_2(OH)_4F_2 \cdot 2H_2O$ LnF_3	[21]
$Y_2(OH)_5Cl{\cdot}1.4H_2O$: Ln^{3+} Ln=Eu, Tb, Dy, Sm	NaF 3 h 180 °C	$Y(OH)_{2.02}F_{0.98}$	[22]
$(Y_{0.95}Eu_{0.05})_2(OH)_5NO_3 \cdot nH_2O$	NH_4F F:Ln= 1 – 66 3 h 90 °C	$Y(OH)_{3-m}F_m$ $K_5Ln_9F_{32}$	[23]

cell parameters were refined as $a = 12.6855(15)$ Å, $b = 7.1671(7)$ Å and $c = 8.4373(9)$ Å. The parameters obtained are smaller than those for pure layered europium hydroxychloride ($a = 12.9155(3)$ Å, $b = 7.3763(1)$ Å, $c = 8.7023(3)$ Å) [26] and larger than those for pure layered yttrium hydroxychloride ($a = 12.6600(1)$ Å, $b = 7.1431(1)$ Å, $c = 8.4209(3)$ Å) [26]. This confirms the formation of layered yttrium-europium hydroxychloride solid solution. According to EDX data, the ratio Y:Eu:Cl=1:0.053(2):0.444(15), which is close to the nominal $(Y_{0.95}Eu_{0.05})_2(OH)_5Cl{\cdot}nH_2O$ composition.

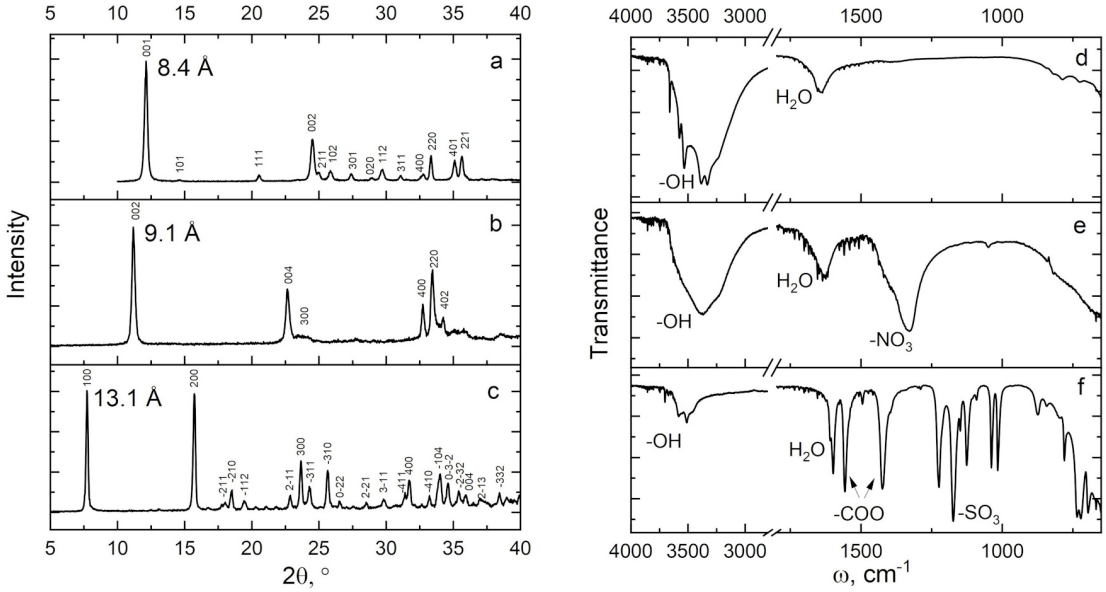

FIG. 1. Diffraction patterns (a–c) and FTIR spectra (d-f) of Eu-doped layered yttrium hydroxychloride (a, d – Cl–LYEuH) and products of its anion-exchange with sodium nitrate (b, e – NO_3–LYEuH) and potassium 4-sulfobenzoate (c, f – 4sb–LYEuH). Diffraction patterns were obtained using CoKα radiation

Figure 1 shows the diffraction patterns of NO_3–LYEuH (Fig. 1b) and 4sb–LYEuH (Fig. 1c) obtained by anion exchange from Cl–LYEuH. X-ray diffraction patterns were indexed according to literature data: NO_3-LYEuH in the *Pc* space group [27] and 4sb–LYEuH in the $P2_1/c$ space group [28]. As a result of anion-exchange reactions, the basal interlayer distance of Eu-doped layered yttrium hydroxide increases from 8.4 Å to 9.1 Å upon intercalation of nitrate anion (Fig. 1b) and to 13.1 Åupon intercalation of 4-sulfobenzoate anion (Fig. 1c). This agrees well with the increasing hydrated radius of anions in the series: chloride- (3.2 Å), nitrate- (3.5 Å) and 4-sulfobenzoate- anion (∼8 Å) [29]. According to EDX data, the europium content is maintained in the range of 0.049 – 0.053 after anion exchange. The ratio S/(Y+Eu)=0.28±0.01, which agrees well with the stoichiometric composition $(Y_{0.95}Eu_{0.05})_2(OH)_5(C_5H_4O_5S)_{0.5} \cdot nH_2O$ for 4sb–LYEuH.

The chloride substitution by nitrate and 4-sulfobenzoate anions is confirmed from the FTIR spectroscopy data in Fig. 1(d–f). On the FTIR spectrum of NO_3–LYEuH (Fig. 1e) a nitrate group stretching vibration band appeared with a maximum at 1624 cm^{-1}. A broad band in the NO_3–LYEuH FTIR spectra with a maximum at 3373 cm^{-1} is attributed to the O–H valence vibrations of intra-layer hydroxyl groups and inter-layer water molecules. In comparison with the FTIR spectrum of Cl–LYEuH (Fig. 1d), this band shows no fine structure, indicating the formation of more hydrogen bonds. A sulfate group stretching vibration band with a maximum at 1172 cm^{-1} and a carboxyl group stretching vibration band with a maximum at 1432 cm^{-1} appeared in the IR spectrum of 4sb–LYEuH (Fig. 1f) [28].

The PXRD results of Eu-doped layered yttrium hydroxychloride fluorination at 150 °C for different durations are presented in Fig. 2. The interaction of Cl–LYEuH with sodium fluoride for 2 h results in a basal interlayer distance decrease from 8.4 Å to 7.4 Å, which is due to the replacement of chloride anions (of 3.2 Å hydrated radius) by smaller fluoride anions (of 2.6 Å hydrated radius) [29] and the formation of stronger and shorter hydrogen bonds involving the fluoride anion in the interlayer space of LRHs [20]. This substitution produces a phase of the $(Y_{0.95}Eu_{0.05})_2(OH)_5F{\cdot}nH_2O$ composition [14]. The diffraction pattern (Fig. 2Aa, marked with an asterisk) of the 2 hours fluorination product shows reflexes of the second phase – hexagonal Eu-doped yttrium hydroxyfluoride (YEuHF) of $Y_{0.95}Eu_{0.05}(OH)_{3-x}F_x$ composition (UCl_3 type system) [30]. This indicates that fluoride anions transform the layered structure by replacing some of the hydroxyl groups in it. Increasing the duration of hydrothermal treatment up to 12 h results in the formation of single-phase YEuHF. Further increase of duration does not affect the phase composition of the products. The matching of some reflections of Cl-LYEuH and YEuHF indicates the maintenance of some atomic planes during fluorination, which allows us to consider this transition as topotactic [15].

For single-phase $Y_{0.95}Eu_{0.05}(OH)_{3-x}F_x$ obtained from Cl–LYEuH, the a and c cell parameters have been calculated in the space group $P6_3/m$ ($Z = 2$) [30]. Both parameters slightly decrease with increasing fluorination duration: $a = 6.0486(14)$ Å, $c = 3.5610(8)$ Å for 12 h; $a = 6.0370(10)$ Å, $c = 3.5576(6)$ Å for 24 h; $a = 6.0348(23)$ Å, $c = 3.5542(15)$ Å for 48 h. Nishizawa et al [30] showed a near linear decrease in the parameter a (6.1976 – 6.0620 Å) with increasing x (0.65 – 1.43) in $Y(OH)_{3-x}F_x$. Decreasing of lattice parameters in our experiment likely indicates that x (in $Y_{0.95}Eu_{0.05}(OH)_{3-x}F_x$) increases with longer fluorination time. Although europium doping usually increases the parameters of yttrium compounds, in our case the parameter a is smaller in absolute value than for the variable composition phase $Y(OH)_{3-x}F_x$ ($x = 0.65$ – 1.43). This may indicate that $x > 1.43$, which is difficult to achieve by synthesis under mild hydrothermal conditions. According to the literature [31], sodium cations also contribute to the stabilization of phase with higher fluorine content, which could increase up to the formation of hexagonal $NaYF_4$ ($a = 5.966$ – 5.976 Å, $c = 3.518$ – 3.531 Å) [32, 33].

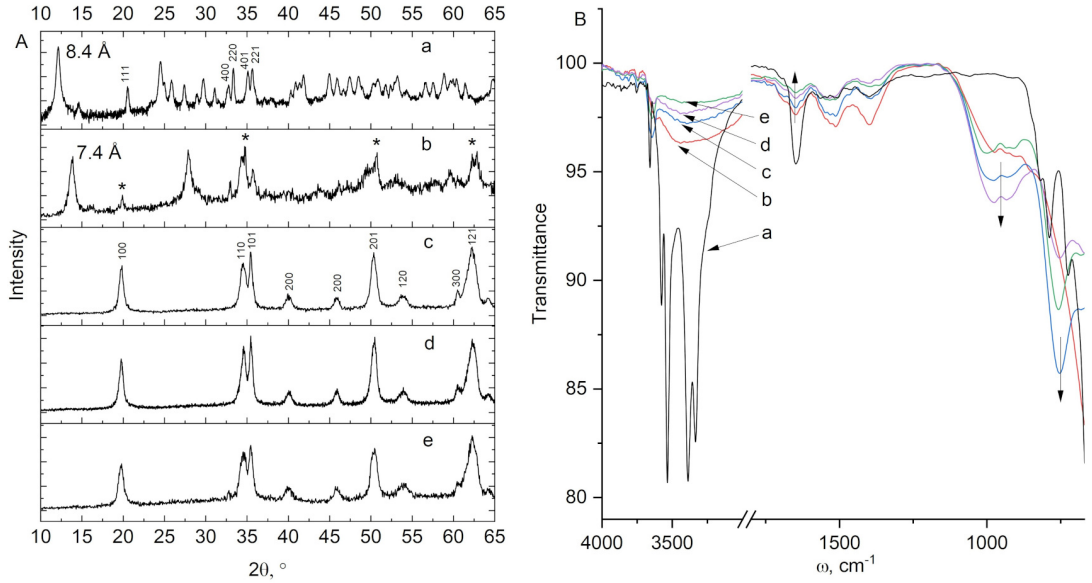

FIG. 2. (A) Diffraction patterns and (B) FTIR spectra of (a) Cl-LYEuH and the products of fluoriation at 150 °C for (b) 2, (c) 12, (d) 24 and (e) 48 h. Diffraction patterns were obtained using CoKα radiation

Additional information on layered structure transformation during Cl–LYEuH fluorination is provided by FTIR spectroscopy data. After fluorination, the intensity of the OH stretching vibration bands (∼3500 cm^{-1}) and HOH deformation vibrations band (∼1650 cm^{-1}) decreases, indicating the substitution of hydroxyl groups by fluoride anions and the destruction of the layered structure, which leads to lower content of interlayer and intralayer water. At the same time, the band of water deformation vibrations (∼1650 cm^{-1}) does not disappear completely, indicating that the composition of YEuHF can be rewritten as $Y_{0.95}Eu_{0.05}(OH)_{3-x}F_x \cdot mH_2O$. At the same time, the bands in the low-frequency region of the spectrum increase in intensity (∼950 cm^{-1} and ∼760 cm^{-1}). Despite the fact that these bands are characteristic for metal hydroxyfluorides [30, 34, 35], their interpretation is not obvious. Wan et al. [35] indicate that peaks at low wavenumbers (1050 – 620 cm^{-1}) are from M–OH and M–F bending mode vibration bands. Klevtsov et al [36] and He et al [34] attribute the absorption bands in the 550 – 800 cm^{-1} region belong to the OH deformation frequencies. In the same region (< 1000 cm^{-1}), rocking modes of the coordinate water molecule can be observed [37].

One of the features of Eu^{3+} luminescence is the sensitivity to the local environment of europium cation [38]. This feature allows us to use luminescence spectroscopy as an additional tool for monitoring the local structure of rare-earth cations during fluorination. Fig. 3 shows the excitation ($\lambda_{em} = 616$ nm) and luminescence spectra ($\lambda_{ex} = 394$ nm) of Cl–LYEuH (Fig. 3a,c) and corresponding YEuHF (150 °C, 48 h) (Fig. 3b,d). The excitation spectra of the samples (Fig. 3a,b) are similar and in good agreement with literature data for layered europium hydroxychloride [25]. The luminescence spectra of the samples (Fig. 3c,d) excited through the maximum emission band $^7F_0$ – $^5L_6$ (394 nm) contain typical Eu^{3+} bands of $^5D_0$ – ^7F_J ($J = 0$ – 4) $f - f$ transitions. The ratio of the intensity ratio of the $^5D_0$ – $^7F_2$ electrodipole transition (hypersensitive to the Eu^{3+} environment) to the intensity of the $^5D_0$ – $^7F_1$ magnetodipole transition (insensitive to the Eu^{3+} environment) increases with decreasing symmetry of the Eu^{3+} environment [39]. In layered rare-earth hydroxychloride structure, rare-earth cations occupy the eight-coordination and nine-coordination positions, in local symmetry groups of C_1 and C_{4v}, respectively [25]. After fluorination, the relative intensity of the $^5D_0$ – $^7F_2$ transition increases, indicating a decrease in the symmetry of the Eu^{3+} environment during fluorination. Apparently, there is a partial substitution of OH- by F- that generates some local distortions and symmetry descent.

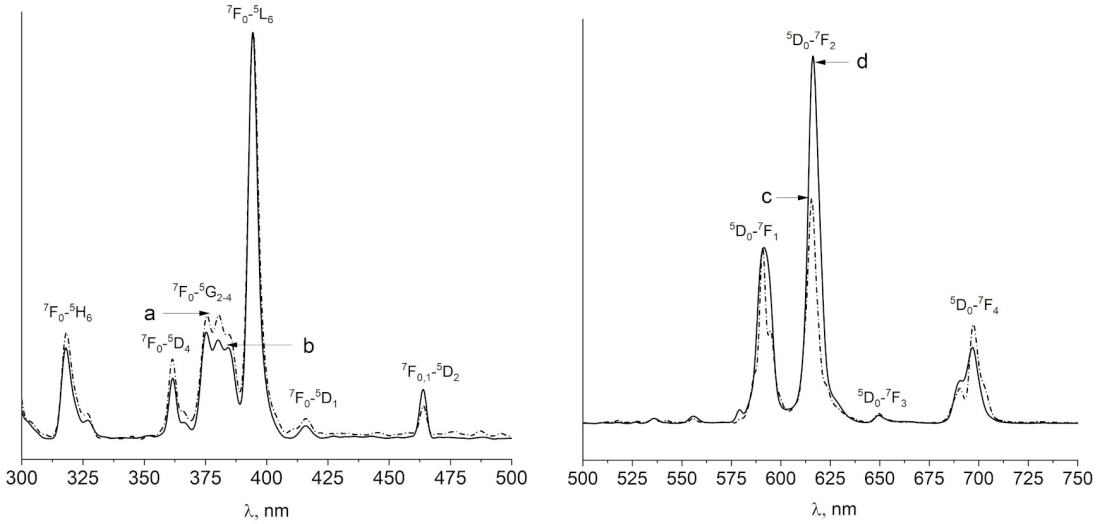

FIG. 3. Excitation (a, b) and emission (c, d) spectra of Cl-LYEuH (a, c) and the product of fluoriation at 150 °C for 48 h (b,d)

Fig. 3a shows the thermal analysis data of Cl–LYEuH and its fluorination products at 150 °C for 2 h (Fig. 3b) and 48 h (Fig. 3c). Based on the mass loss in the first stage (25 – 220 °C), the hydrate water content of the Cl–LYEuH was refined as $(Y_{0.95}Eu_{0.05})_2(OH)_5Cl{\cdot}1.6H_2O$. With increasing fluorination duration, a decrease in the total mass loss was observed, which is in good agreement with the decrease in the water content and hydroxyl groups in $Y_{0.95}Eu_{0.05}(OH)_{3-x}F_x \cdot mH_2O$ compared to $(Y_{0.95}Eu_{0.05})_2(OH)_5Cl{\cdot}1.6H_2O$. Fig. 3d–f also shows differential thermal analysis data, which indicate a shift in the dehydroxylation temperature (220 – 350 °C) during the fluorination of $(Y_{0.95}Eu_{0.05})_2(OH)_5Cl{\cdot}1.6H_2O$. For Cl–LYEuH, the temperature of the maximum dehydroxylation rate is 329 °C. After fluorination of Cl–LYEuH for 2 hours, the temperature decreases to 270 °C. This sample corresponds mainly to the $(Y_{0.95}Eu_{0.05})_2(OH)_5F{\cdot}nH_2O$ phase (Fig. 2b), which seems to be characterized by a smaller number of free hydroxyl groups displaced by the fluoride anion in interlayer space. The appearance of freer hydroxyl groups contributes to a lower removal temperature. Fluorination of Cl–LYEuH for 48 h results in the formation of the YEuHF phase, in which the hydroxyl groups are firmly bonded in the crystal structure. The larger number of halide ions and stronger OH-Hal hydrogen bonds in the case of $Y_{0.95}Eu_{0.05}(OH)_{3-x}F_x \cdot mH_2O$ compared to $(Y_{0.95}Eu_{0.05})_2(OH)_5Cl{\cdot}1.6H_2O$ contribute to the increase of the dehydroxylation temperature up to 346 °C (Fig. 4f).

The results of PXRD and FTIR spectroscopy for the NO_3–LYEuH fluorination at 150 °C are presented in Fig. 9 (see Appendix). As in the case of Cl–LYEuH (Fig. 2), fluorination occurs through the formation of the $(Y_{0.95}Eu_{0.05})_2(OH)_5F{\cdot}nH_2O$ phase (Fig. 9Ab) and is completed by the $Y_{0.95}Eu_{0.05}(OH)_{3-x}F_x \cdot mH_2O$ formation within

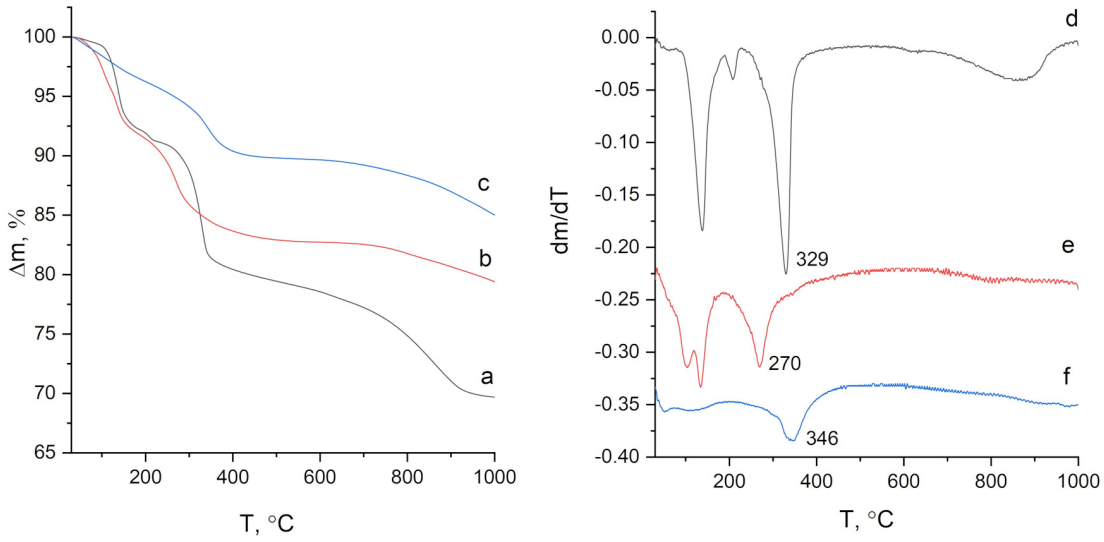

FIG. 4. Mass loss curves (a–c) and their derivatives (d–f) for Cl–LYEuH (a,d) and the products of fluoriation at 150 °C for 2(b,e) and 48 h (c,f)

12 h (Fig. 9Ac). This is confirmed by FTIR spectroscopy data (Fig. 9B). After NO_3–LYEuH fluorination, the nitrate stretching vibration band with a maximum at 1335 cm^{-1} completely disappears, and the intensity of the OH stretching vibration bands (3400 cm^{-1}) and the water deformation vibrations (1650 cm^{-1}) decreases. However, in comparison with the FTIR data for Cl–LYEuH fluorination (Fig. 2), there is a shift in the bands of deformation OH vibrations, which may indicate the formation of oriented attachment structures (mesocrystals) [34]. The disappearance of the narrow OH stretching vibration band of hydroxyl group (> 3600 cm^{-1}) indicates a high fluorination efficiency – the full replacement of free hydroxyl groups by fluoride ions. The higher efficiency of NO_3-LYEuH fluorination compared to Cl–LYEuH is indicated by the smaller cell parameter a for YEuHF: $a = 6.0343(18)$ Å, $c = 3.5546(10)$ Å for 12 h fluorination and $a = 6.0249(11)$ Å, $c = 3.5553(5)$ Å for 48 h fluorination.

At 150 °C there are no significant differences in the fluorination rates of Cl–LYEuH and NO_3–LYEuH. However, the situation changes when the temperature is reduced to 100 °C (Fig. 5). As the temperature decreases, the rate of fluorination slows down in both cases. After 2 h of Cl–LYEuH fluorination, it was possible to obtain a single-phase of $(Y_{0.95}Eu_{0.05})_2(OH)_5F{\cdot}nH_2O$ without impurity of $Y_{0.95}Eu_{0.05}(OH)_{3-x}F_x \cdot mH_2O$ (Fig. 5a). The NO_3–LYEuH fluorination rate at 100 °C is markedly higher than that for Cl-LYEuH. The single phase $Y_{0.95}Eu_{0.05}(OH)_{3-x}F_x \cdot mH_2O$ is formed within 24 h of NO_3–LYEuH fluorination (Fig. 5d), while for Cl–LYEuH fluorination products, a mixture of $Y_{0.95}Eu_{0.05}(OH)_{3-x}F_x \cdot mH_2O$ and $(Y_{0.95}Eu_{0.05})_2(OH)_5F{\cdot}nH_2O$ phases is retained for the same time (Fig. 5b). Thus, it can be concluded that the NO_3–LYEuH fluorination rate is higher than that for Cl–LYEuH.

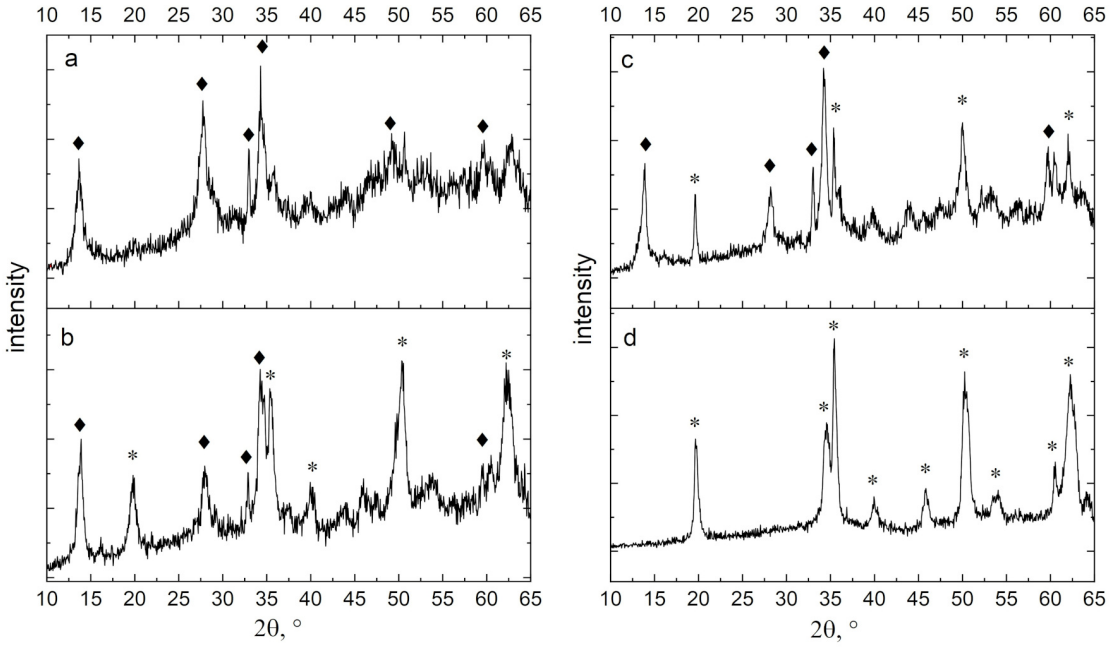

FIG. 5. X-ray diffraction patterns of (a,b) Cl–LYEuH and (c,d) NO_3–LYEuH after fluoration at 100 °C for (a,c) 2 h and (b,d) 24 h. ♦ – $(Y_{0.95}Eu_{0.05})_2(OH)_5F{\cdot}nH_2O$ phase, ∗ – $Y_{0.95}Eu_{0.05}(OH)_{3-x}F_x{\cdot}mH_2O$ phase. Diffraction patterns were obtained using CoKα radiation

The 4sb–LYEuH fluorination process differs significantly from the Cl–LYEuH and NO_3–LYEuH fluorination. According to PXRD (Fig. 6), the formation of single-phase $Y_{0.95}Eu_{0.05}(OH)_{3-x}F_x \cdot mH_2O$ is observed within 2 h. The $(Y_{0.95}Eu_{0.05})_2(OH)_5F{\cdot}nH_2O$ phase didn't appear during the 4sb–LYEuH fluorination process, which indicates different fluorination mechanism compared to the Cl–LYEuH and NO_3–LYEuH fluorination. As well as the rates, the fluorination efficiency also increases for 4sb–LYEuH, as indicated by the decrease of the cell parameters of $Y_{0.95}Eu_{0.05}(OH)_{3-x}F{\cdot}mH_2O$ to the minimum values of $a = 6.0041(10)$ Å, $c = 3.5463(6)$ (4sb–LYEuH fluorination at 150 °C for 48 h).

According to the FTIR spectroscopy data (Fig. 6B), 4sb–LYEuH fluorination for 2 – 12 h leads to a significant decrease in the OH stretching vibration band and 4-sulfobenzoate anion characteristic vibrations band intensities. This indicates the retention of trace amounts of organic anion in the fluorination products for 2 – 12 h. These bands disappear completely when the fluorination duration reaches 24 h, indicating the formation of a pure product. Note that water is practically absent in the fluorination products of 4sb–LYEuH, as indicated by the very low intensity of HOH vibration band in the region of 1650 cm^{-1}. This is in good agreement with the difference in the structure of 4sb–LYEuH [28] and Cl–LYEuH [26] or NO_3–LYEuH [27]. Firstly, 4sb–LYEuH has lower water per rare-earth atom ratio, and secondly, water molecules in 4sb–LYEuH interlayer space do not coordinate to the rare-earth atoms [28]. That makes inclusion of water molecules in fluorinated structure very unlikely. In the case of Cl–LYEuH or NO_3–LYEuH, water molecules are involved

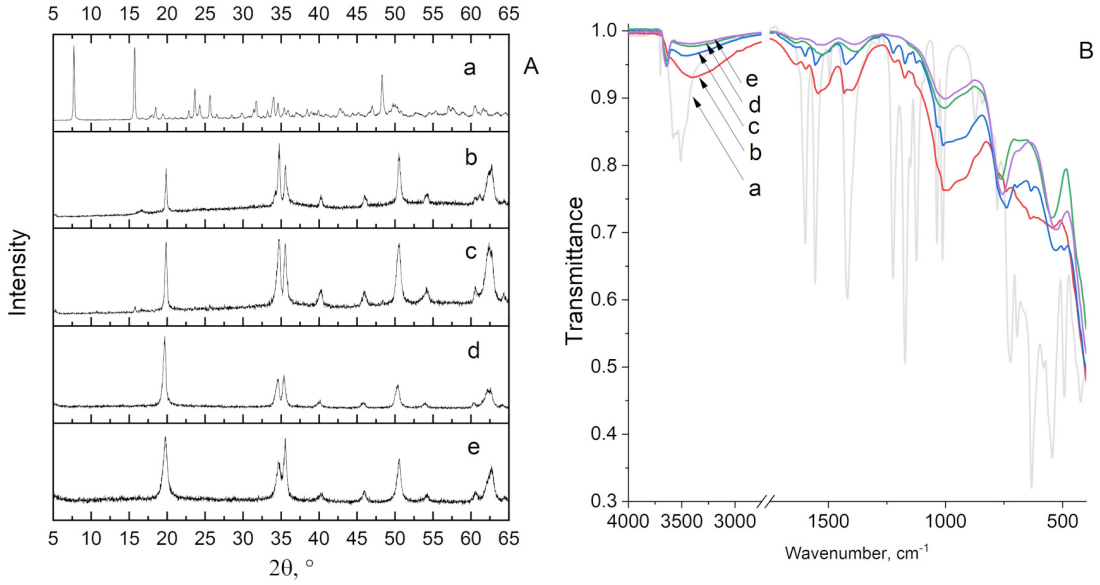

FIG. 6. (A) Diffraction patterns and (B) FTIR spectra of (a) 4sb–LYEuH and the products of fluoriation at 150 °C for (b) 2, (c) 12, (d) 24 and (e) 48 h. Diffraction patterns were obtained using CoKα radiation

in the coordination sphere of rare-earth atoms [26,27], which significantly increases the probability of their capture during fluorination.

Figure 7a shows the content of elements (Y, Eu, F, Na) in the fluorination final products (duration of 48 h) of Cl–LYEuH, NO_3–LYEuH, and 4sb–LYEuH. Taking into account presence of sodium ions, the composition of fluorinated materials can be rewritten as $Na_yY_{0.95}Eu_{0.05}(OH)_{3+y-x}F_x \cdot mH_2O$. According to EDX data for all compositions, $x \sim 3$, and $y \sim 0.2$. This indicates that the anionic composition does not affect the composition of the formed product. The anionic composition affects the fluorination rate, as can be seen in Fig. 7b, the rate increases in the series of anions: chloride, nitrate and 4-sulfobenzoate. The increase in the rate can be related to the increase in the interlayer distance in the corresponding series. The interlayer distance can be calculated by subtracting the thickness of the metal-hydroxide layer (5.5 Å) from the basal interlayer distance (Fig. 1) [9]. The corresponding value increases in the series of intercalated anions: chloride (2.9 Å), nitrate (3.6 Å) and 4-sulfobenzoate (7.6 Å). Apparently, increasing the interplanar distance accelerates the diffusion of fluoride anions into the yttrium-europium layered hydroxide structure, thereby increasing the contact area and interaction rate. In the case of 4-sulfobenzoate, the interplanar distance was so high that the formation of the intermediate phase of $(Y_{0.95}Eu_{0.05})_2(OH)_5F{\cdot}nH_2O$ was not observed.

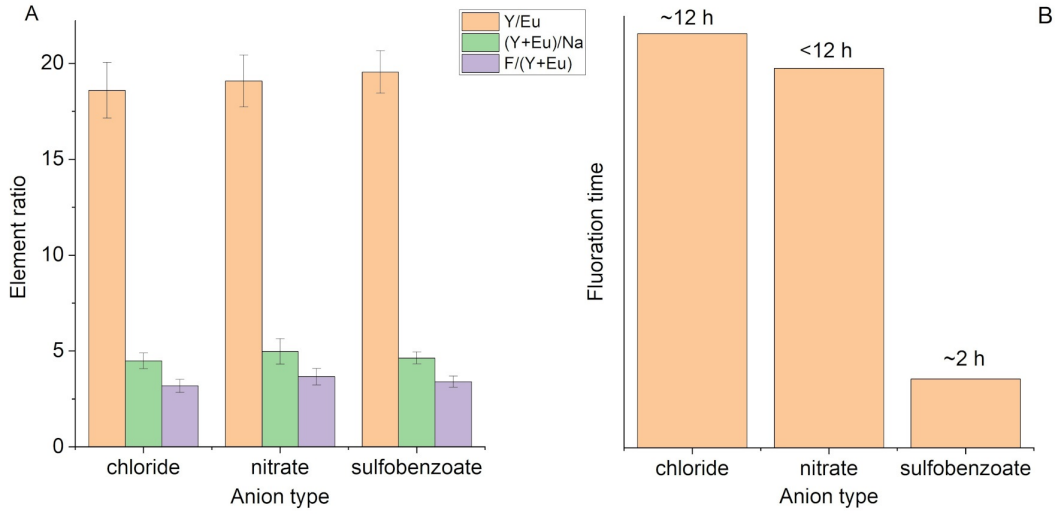

FIG. 7. (A) EDX data for Cl–LYEuH, NO_3–LYEuH, and 4sb–LYEuH after fluorination at 150 °C for 48 h. (B) Approximate duration of formation of single-phase $NayY_{0.95}Eu_{0.05}(OH)_{3+y-x}F_x \cdot mH_2O$ from Cl–LYEuH, NO_3–LYEuH, and 4sb–LYEuH at 150 °C

In order to investigate the mechanism of fluorination, the morphology of the obtained $Na_yY_{0.95}Eu_{0.05}(OH)_{3+y-x}F_x \cdot mH_2O$ particles was studied by scanning electron microscopy (Fig. 8). In all cases, fluorination results in the formation of rod-like nanoparticles of $Na_yY_{0.95}Eu_{0.05}(OH)_{3+y-x}F_x \cdot mH_2O$, whose size and shape differ depending on the anionic composition of the precursor. In the case of Cl–LYEuH and NO_3–LYEuH fluorination, the morphology of the lamellar particles is partially preserved, indicating a topotactic reaction mechanism in these cases [15–17]. The tendency to morphology preservation is more remarkable for Cl–LYEuH, which can be explained by the lowest fluorination rate. In the case of NO_3–LYEuH fluorination, the laminae are completely fragmented into rod-like particles, forming aggregates of interlocked particles like "bamboo mat". Such structures are similar to the oriented attachment structures described for yttrium hydroxyfluorides [34, 40].

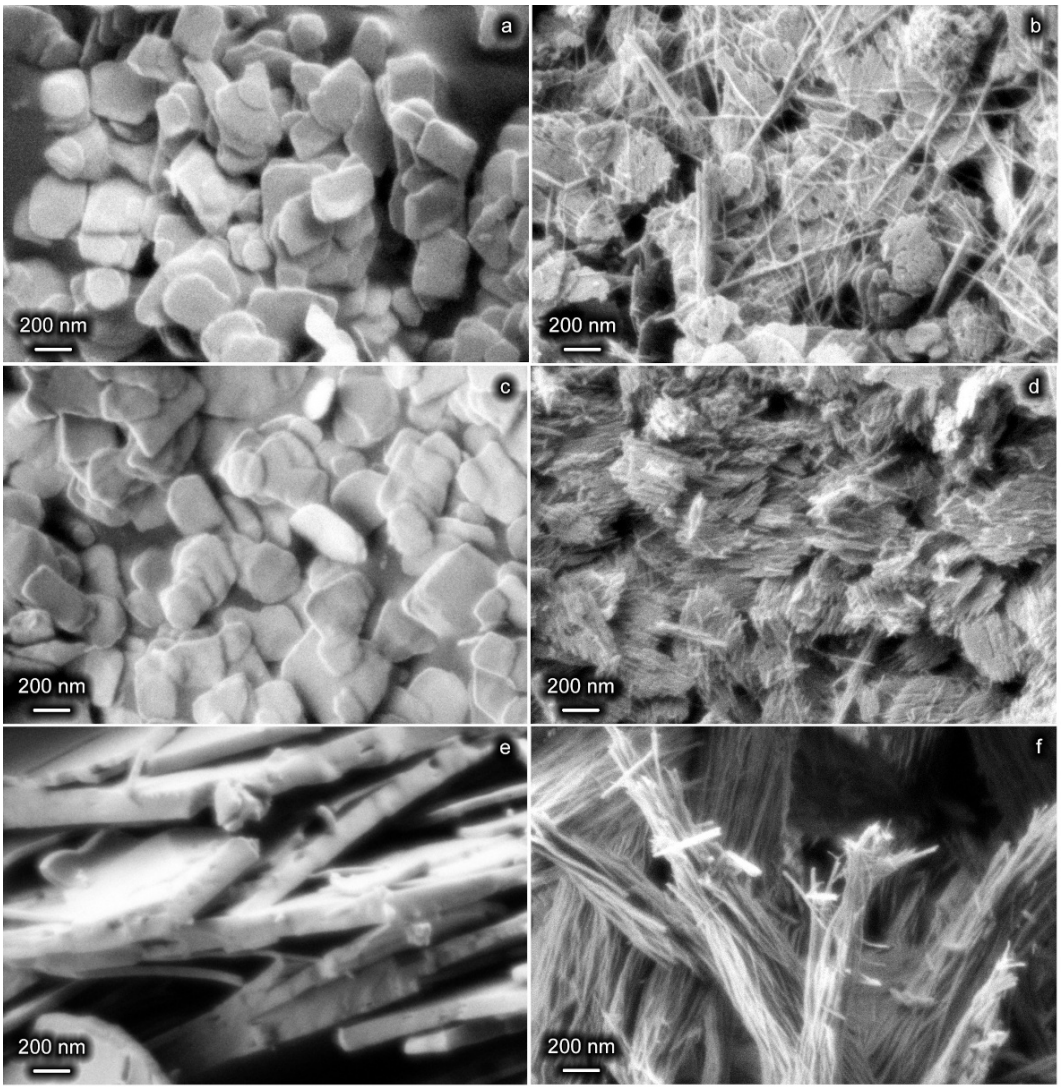

FIG. 8. SEM images of (a,b) Cl–LYEuH, (c,d) NO_3–LYEuH, and (e,f) 4sb–LYEuH before (a,c,e) and after (b,d,f) their fluorination at 150 °C for 48 h

It should be noted that chloride anion is exchanged for nitrate anion at room temperature without change in the morphology of the lamellar particles (Fig. 8a,c). When the chloride anion is exchanged for 4-sulfobenzoate anion under hydrothermal conditions, the size of lamellar particles increases significantly (Fig. 8e), indicating the active participation of dissolution- recrystallization processes during ion exchange involving 4-sulfobenzoate anion. Despite the larger particle size, and thus slower diffusion of fluoride anions, the 4sb–LYEuH fluorination occurs most rapidly, indicating different fluorination mechanisms for 4sb–LYEuH and Cl–LYEuH or NO_3–LYEuH. In the case of 4sb–LYEuH fluorination, sheaves of rod-like particles are formed without retaining a lamellar morphology, which agrees well with the mechanism proposed earlier in the literature for the fluorination of layered yttrium hydroxide [17]. This mechanism involves stages of ion exchange, exfoliation, oriented attachment, and Ostwald ripening. Exfoliation prevents the lamellar morphology from remaining as in the case of Cl–LYEuH or NO_3–LYEuH. Thus, the anionic composition of the LRHs determines both the rate and mechanism of their fluorination process.

4. Conclusions

The interaction of Eu-doped layered yttrium hydroxide with aqueous solutions of sodium fluoride yielded the Eu-doped yttrium hydroxyfluoride phase of $Na_yY_{0.95}Eu_{0.05}(OH)_{3+y-x}F_x \cdot mH_2O$ ($x \sim 3$, $y \sim 0.2$) composition. For the first time, rare-earth hydroxyfluoride was prepared from layered rare-earth hydroxide intercalated with an organic (4-sulfobenzate) anion. It is shown that the increase in the reaction temperature (from 100 to 150 °C) and the increase in the interlayer distance of layered hydroxide lead to higher rate of fluorination. The formation rate of Eu-doped yttrium hydroxyfluoride increases in the following series of intercalated anions: chloride-, nitrate-, and 4-sulfobenzoate-anions. In the same series, the tendency to retain the morphology of lamellar particles after fluorination decreases. The high vs low fluorination rate, the absence vs presence of the intermediate $(Y_{0.95}Eu_{0.05})_2(OH)_5F{\cdot}nH_2O$ phase and the sheaf-like vs laminar morphology of the particles indicate difference in fluorination mechanism of Eu-doped layered hydroxysulfobenzoate and Eu-doped layered yttrium hydroxynitrate or hydroxychloride.

Appendix

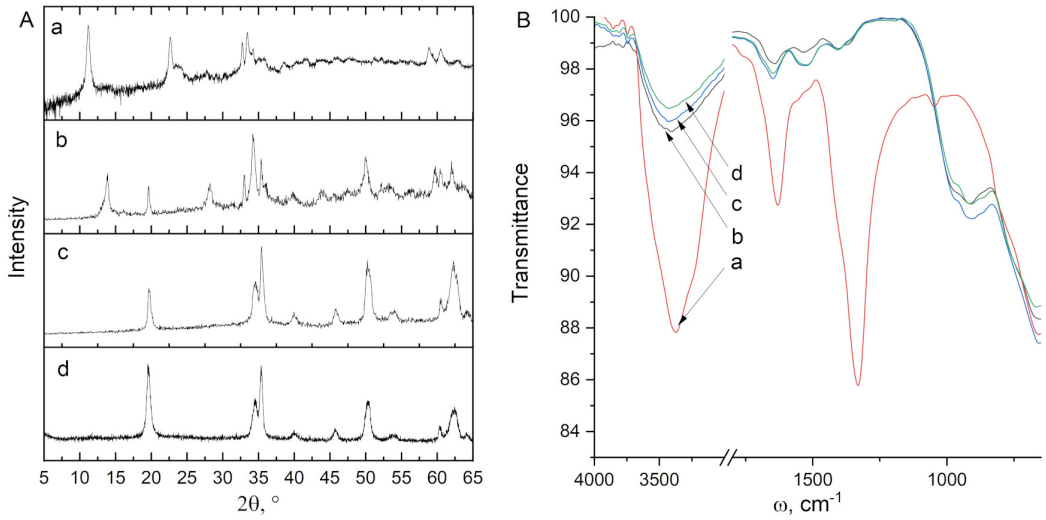

FIG. 9. (A) Diffraction patterns and (B) FTIR spectra of (a) NO_3–LYEuH and the products of fluoriation at 150 °C for (b) 2, (c) 12, and (d) 48 h.

References

[1] Yao X., Wang R., Zhao J., Liu F., Jin Z., Wang Z., Wang F., Liu J., Wu. L. An overview of metal hydroxyfluoride–A novel semiconductor material *ChemPhysMater*, 2023, P. S2772571523000359.

[2] Serna-Gallén P., Beltrán-Mir H., Cordoncillo E. The pH-dependent reactions in the sonochemical synthesis of luminescent fluorides: The quest for the formation of KY_3F_{10} crystal phases. *Ultrason. Sonochem.*, 2022, **87**, P. 106059.

[3] Zhu L.-L., Liu B.-Q., Chen X.-Y., Feng A., Zhang Z.-J., Zhao J.-T. Synthesis, characterization and luminescence properties of $NaY(OH)_xF_{4-x}$: Sm with spindle shape. *Mater. Res. Bull.*, 2015, **68**, P. 289–294.

[4] Xu J., Zhu T., Chen X., Zhao D., Li Y., Zhang L., Bi N., Gou J., Jia L. Tri-channel tubular lanthanide nanocomposites for multimodal anti-counterfeiting. *J. Lumin.*, 2023, **256**, P. 119647.

[5] Lima E., Pfeiffer H., Flores J. Some consequences of the fluorination of brucite-like layers in layered double hydroxides: Adsorption. *Appl. Clay Sci.* 2014, **88-89**, P. 26–32.

[6] Booster J.L., Van Sandwijk A., Reuter M.A. Conversion of magnesium fluoride to magnesium hydroxide. *Miner. Eng.*, 2003, **16**(3), P. 273–281.

[7] Timofeeva E., Orlovskaya E., Popov A., Shaidulin A., Kuznetsov S., Alexandrov A., Uvarov O., Vainer Y., Silaev G., Rähn M., Tamm A., Fedorenko S., Orlovskii Y. The Influence of Medium on Fluorescence Quenching of Colloidal Solutions of the Nd^{3+}: LaF_3 Nanoparticles Prepared with HTMW Treatment. *Nanomaterials*, 2022, **12**(21), P. 3749.

[8] F. Gándara, J. Perles, N. Snejko, M. Iglesias, B. Gómez-Lor, E. Gutiérrez-Puebla, M.Á. Monge. Layered Rare-Earth Hydroxides: A Class of Pillared Crystalline Compounds for Intercalation Chemistry. *Angew. Chem. Int. Ed.*, 2006, **45**(47), P. 7998–8001.

[9] Yapryntsev A.D., Baranchikov A.E., Ivanov V.K. Layered rare-earth hydroxides: a new family of anion-exchangeable layered inorganic materials. *Russ. Chem. Rev.*, 2020, **89**(6), P. 629–666.

[10] Zhang H., Chen T., Qin S., Huang J., Wu X. Fabrication of REVO 4 films *via* sacrificial conversion from layered rare-earth hydroxide (LRH) films: the investigation of the transition mechanism and their photoluminescence. *Dalton Trans*, 2022, **51**(14), P. 5577–5586.

[11] Wang X., Sun M., Hu Z., Du P., Liu W., Zhang F., Li J.-G. Synthesis of $NaLn(WO_4)_2$ phosphors via a new phase-conversion protocol and investigation of up/down conversion photoluminescence. *Adv. Powder Technol.*, 2020, **31**(10), P. 4231–4240.

[12] Wang Z., Li J.-G.G., Zhu Q., Li X., Sun X. Sacrificial conversion of layered rare-earth hydroxide (LRH) nanosheets into $(Y_{1-x}Eu_x)PO_4$ nanophosphors and investigation of photoluminescence. *Dalton Trans*, 2016, **45**(12), P. 5290–5299.

[13] Wang Z., Li J.-G., Zhu Q., Li X., Sun X. Hydrothermal conversion of layered hydroxide nanosheets into $(Y_{0.95}Eu_{0.05})PO_4$ and $(Y_{0.96-x}Tb_{0.04}Eu_x)PO_4$ ($x = 0$–0.10) nanocrystals for red and color-tailorable emission. *RSC Adv.*, 2016, **6**(27), P. 22690–22699.

[14] Li J., Li J.-G., Zhu Q., Sun X. Room-temperature fluorination of layered rare-earth hydroxide nanosheets leading to fluoride nanocrystals and elucidation of down-/up-conversion photoluminescence. *Mater. Des.*, 2016, **112**, P. 207–216.
[15] Feng Y., Shao B., Song Y., Zhao S., Huo J., Lü W., You H. Fast synthesis of β-$NaYF_4$: Ln^{3+} (Ln = Yb/Er, Yb/Tm) upconversion nanocrystals via a topotactic transformation route. *CrystEngComm.*, 2016, **18**(39), P. 7601–7606.
[16] Xu Z., Tang G., Meng W., Feng H., Zhang Z., Zhao J. Controlled synthesis of hydrophilic yttrium-based fluorids by transformation from layered rare-earth hydroxides. *Opt. Mater. Elsevier B.V.*, 2020, **108**(May), P. 110220.
[17] Shao B., Zhao Q., Lv W., Jiao M., Lü W., You H. Novel Two-step topotactic transformation synthetic route towards monodisperse LnOF: Re,3+ (Ln = Y, Pr-Lu) Nanocrystals with down/upconversion luminescence properties. *Adv. Opt. Mater.*, 2015, **3**(4), P. 583–592.
[18] Omwoma S., Stephen Odongo A., Otieno Z., Lagat S., Lalah J.O. Layered Rare-Earth Hydroxide Unilameller Nanosheets: Synthesis, Characterization, and Adsorption. *J. Chem.*, 2020, **2020**, P. 8923871.
[19] Liu S., Li J.G., Liu W., Cui H., Liu M., Chen J., Zhu H., Li X., Sun X. A novel method for improving particle growth and photoluminescence through F- substituting for gallery NO^{3-} in layered Y/Eu hydroxides. *Chem. Eng. J. Elsevier*, 2020, **380**, P. 122618.
[20] Wu X., Li J.-G.J.G.J.-G.J.G., Zhu Q., Liu W., Li J.-G.J.G.J.-G.J.G., Li X., Sun X., Sakka Y. One-step freezing temperature crystallization of layered rare-earth hydroxide (Ln(2)(OH)(5)NO(3 center dot)nH(2)O) nanosheets for a wide spectrum of Ln (Ln = Pr-Er, and Y), anion exchange with fluorine and sulfate, and microscopic coordination probed via. *J. Mater. Chem. C.*, 2015, **3**(14), P. 3428–3437.
[21] Wang X., Hu Z., Sun M., Du P., Liu W., Huang S., Li J.G. Phase-conversion synthesis of LaF_3:Yb/RE (RE = Ho, Er) nanocrystals with $Ln_2(OH)_4SO_4 \cdot 2H_2O$ type layered compound as a new template, phase/morphology evolution, and upconversion luminescence. *J. Mater. Res. Technol. Korea Institute of Oriental Medicine*, 2020, **9**(5), P. 10659–10668.
[22] Dong J., Wang X., Xiong H., Song H., Wu R., Gan S. A novel synthetic route towards monodisperse yttrium hydroxide fluoride by anion exchange and luminescence properties. *Opt. Laser Technol.*, 2019, **111**, P. 372–379.
[23] Li J., Wang X., Zhu Q., Kim B.-N., Sun X., Li J.-G. Interacting layered hydroxide nanosheets with KF leading to Y/Eu hydroxyfluoride, oxyfluoride, and complex fluoride nanocrystals and investigation of photoluminescence. *RSC Adv.*, 2017, **7**(83), P. 53032–53042.
[24] Liu B.-Q., Guo K., Wang J., Zhang Z.-J., Tao Y., Huang Y., Zhao J.-T. Mild hydrothermal synthesis and photoluminescence of needle-like $Y(OH)_{1.1}F_{1.9}$:Tb^{3+}. *Mater. Lett.*, 2013, **100**, P. 245–247.
[25] Geng F. et al. New layered rare-earth hydroxides with anion-exchange properties. *Chem. - Eur. J.*, 2008, **14**(30), P. 9255–9260.
[26] Geng F., Matsushita Y., Ma R., Xin H., Tanaka M., Izumi F., Iyi N., Sasaki T. General synthesis and structural evolution of a layered family of $Ln_8(OH)_{20}Cl_4 \cdot nH_2O$ (Ln = Nd, Sm, Eu, Gd, Tb, Dy, Ho, Er, Tm, and Y). *J. Am. Chem. Soc.*, 2008, **130**(48), P. 16344–16350.
[27] Geng F., Matsushita Y., Ma R., Xin H., Tanaka M., Iyi N., Sasaki T., Renzhi M., Xin H., Tanaka M., Lyi N., Sasaki T., Ma R., Xin H., Tanaka M., Iyi N., Sasaki T. Synthesis and properties of well-crystallized layered rare-earth hydroxide nitrates from homogeneous precipitation. *Inorg. Chem.*, 2009, **48**(14), P. 6724–6730.
[28] Yapryntsev A., Abdusatorov B., Yakushev I., Svetogorov R., Gavrikov A., Rodina A., Fatyushina Y., Baranchikov A., Zubavichus Y., Ivanov V. Eu-Doped layered yttrium hydroxides sensitized by a series of benzenedicarboxylate and sulphobenzoate anions. *Dalton Trans.*, 2019, **48**(18).
[29] Marcus Y. Ionic radii in aqueous solutions. *Chem. Rev.*, 1988, **88**(8), P. 1475–1498.
[30] Nishizawa H., Okumoto K., Mitsushio T. Preparation and thermal decomposition of yttrium hydroxide fluorides. *J. Solid State Chem.*, 1991, **92**(2), P. 370–379.
[31] Grzechnik A., Bouvier P., Mezouar M., Mathews M.D., Tyagi A.K., Köhler J. Hexagonal $Na_{1.5}Y_{1.5}F_6$ at High Pressures. *J. Solid State Chem.*, 2002, **165**(1), P. 159–164.
[32] Fedorov P., Mayakova M., Voronov V., Baranchikov A., Ivanov V. Preparation of "NaREF4" phases from the sodium nitrate melt. *J. Fluor. Chem.*, 2019, **218**, P. 69–75.
[33] Krämer K.W., Biner D., Frei G., Güdel H.U., Hehlen M.P., Lüthi S.R. Hexagonal Sodium Yttrium Fluoride Based Green and Blue Emitting Upconversion Phosphors. *Chem. Mater.*, 2004, **16**(7), P. 1244–1251.
[34] He X., Yan B. Yttrium hydroxide fluoride based monodisperse mesocrystals: additive-free synthesis, enhanced fluorescence properties, and potential applications in temperature sensing. *CrystEngComm.*, 2015, **17**(3), P. 621–627.
[35] Wan S., Qi J., Zhang W., Wang W., Zhang S., Liu K., Zheng H., Sun J., Wang S., Cao R. Hierarchical Co(OH)F Superstructure Built by Low-Dimensional Substructures for Electrocatalytic Water Oxidation. *Adv. Mater.*, 2017, **29**(28), P. 1700286.
[36] Klevtsov P.V., Bembel' V.M., Grankina Z.A. Crystalline hydroxychlorides, $Ln(OH)_2Cl$, of the rare-earth elements of the cerium group. *J. Struct. Chem.*, 1970, **10**(4), P. 543–547.
[37] Nakamoto K. *Applications in Coordination Chemistry. Infrared and Raman Spectra of Inorganic and Coordination Compounds*. John Wiley & Sons, Inc., 2008, P. 1–273.
[38] Utochnikova V.V. The use of luminescent spectroscopy to obtain information about the composition and the structure of lanthanide coordination compounds. *Coord. Chem. Rev.*, 2019, **398**, P. 113006.
[39] Binnemans K. Interpretation of europium(III) spectra. *Coord. Chem. Rev.*, 2015, **295**, P. 1–45.
[40] Zhuang J., Yang X., Fu J., Liang C., Wu M., Wang J., Su Q. Monodispersed β-$NaYF_4$ Mesocrystals: In Situ Ion Exchange and Multicolor Up- and Down-Conversions. *Cryst. Growth Des.*, 2013, **13**(6), P. 2292–2297.

Submitted 19 December 2023; revised 4 February 2024; accepted 12 February 2024

Information about the authors:

Zhanbo Liu – Shenzhen MSU-BIT University, Shenzhen, PRC; ORCID 0009-0007-5390-2154; sdbzlzb@126.com

Svetlana V. Golodukhina – Shenzhen MSU-BIT University, Shenzhen, PRC; Kurnakov Institute of General and Inorganic Chemistry of the Russian Academy of Sciences, Moscow, Russia; ORCID 0000-0001-9317-1340; brightorangedandelion@gmail.com

Svetlana V. Kameneva – Shenzhen MSU-BIT University, Shenzhen, PRC; ORCID 0000-0003-4860-4973; kamenevasvetlanav@gmail.com

Alexey D. Yapryntsev – Shenzhen MSU-BIT University, Shenzhen, PRC; Kurnakov Institute of General and Inorganic Chemistry of the Russian Academy of Sciences, Moscow, Russia; ORCID 0000-0001-8166-2476; yapryntsev@igic.ras.ru

Conflict of interest: the authors declare no conflict of interest.